

Doping and dimensionality effects on the core-level spectra of layered ruthenates

Haizhong Guo,^{1,2} Yi Li,¹ Darwin Urbina,³ Biao Hu,¹ Rongying Jin,¹ Tijiang Liu,⁴ David Fobes,⁴ Zhiqiang Mao,⁴ E. W. Plummer,¹ and Jiandi Zhang^{1,*}

¹Department of Physics and Astronomy, Louisiana State University, Baton Rouge, Louisiana 70803, USA

²Beijing National Laboratory for Condensed Matter Physics, Institute of Physics, Chinese Academy of Sciences, Beijing 100190, People's Republic of China

³Department of Physics, Florida International University, Miami, Florida 33199, USA

⁴Physics Department, Tulane University, New Orleans, Louisiana 70118, USA

(Received 29 September 2009; revised manuscript received 12 March 2010; published 26 April 2010)

Core-level spectra of the Mn-doped $\text{Sr}_3\text{Ru}_2\text{O}_7$ and $\text{Sr}_{n+1}\text{Ru}_n\text{O}_{3n+1}$ ($n=1, 2$, and 3) crystals are investigated with x-ray photoelectron spectroscopy. Doping of Mn to $\text{Sr}_3\text{Ru}_2\text{O}_7$ considerably affects the distribution of core-level spectral weight. The satellite of Ru $3d$ core levels exhibits a substantial change with doping, indicating an enhanced electron localization across the doping-induced metal-insulator transition. However, the Ru $3p$ core levels remain identical with Mn doping, thus showing no sign of doping-induced multiple Ru valences. In the $\text{Sr}_{n+1}\text{Ru}_n\text{O}_{3n+1}$ ($n=1, 2$, and 3), the Ru $3d$ core-level spectra are similar, indicating that the chemical bonding environment around Ru ions remains the same for different layered compounds. While the Sr $3d$ shallow core levels shift to higher binding energy with increasing n , suggesting their participation in Sr-O bonding with structural evolution.

DOI: [10.1103/PhysRevB.81.155121](https://doi.org/10.1103/PhysRevB.81.155121)

PACS number(s): 71.30.+h, 79.60.-i, 71.28.+d

I. INTRODUCTION

The layered ruthenates of the Ruddlesden-Popper series $\text{Sr}_{n+1}\text{Ru}_n\text{O}_{3n+1}$ (see Fig. 1), where n ($n=1, 2, 3, \dots, \infty$) is the number of layers of corner-sharing RuO_6 octahedra per formula unit, display a remarkable array of complex electronic and magnetic properties.^{1,2} The complexity, which is intimately related to the coexistence of competing nearly degenerate states which couple simultaneously active degrees of freedom: charge, lattice, orbital, and spin states, is directly responsible for their tunability. Specifically, the properties of $\text{Sr}_{n+1}\text{Ru}_n\text{O}_{3n+1}$ exhibit strong dependence on the number (n) of RuO_6 octahedral layers in crystal structure, reflecting the effect of dimensionality in the system. Single-layered Sr_2RuO_4 ($n=1$), as the most two-dimensional-like compound in the perovskite series, is an unconventional superconductor with possible spin-triplet pairing.^{1,3-5} The bilayered $\text{Sr}_3\text{Ru}_2\text{O}_7$ ($n=2$) shows behavior consistent with proximity to a metamagnetic quantum critical point.⁶ The magnetic ground state of the triple-layer $\text{Sr}_4\text{Ru}_3\text{O}_{10}$ ($n=3$) is poised between an itinerant metamagnetic and itinerant ferromagnetic state.⁷⁻⁹ SrRuO_3 ($n=\infty$), regarded as a three-dimensional compound, is an itinerant ferromagnet with unusual transport characteristic.^{10,11} On the other hand, the replacement of Sr with Ca (Ref. 12) or Ru with other transition-metal ions such as Mn (Refs. 13 and 14) causes a metal-to-insulator transition (MIT), reflecting the manifestation on transport property by replacing ions with different sizes. Especially, the dilute Mn doping provides a remarkably effective pathway of tuning on electronic structure beyond disorder-induced electron localization.¹⁴ However, the nature of such a doping-induced MIT is still under investigation.

X-ray photoelectron spectroscopy (XPS) has been widely used to study the chemical environment and the electronic structure of materials. In particular, the satellite structures in

the core-level photoemission spectra provide important information about the interactions of electrons in correlated systems such as transition-metal oxides.¹⁵ One example is the XPS study of various ruthenates, where Ru $3d$ core-level XPS spectra have satellites which are suggested as a result of two different screening mechanisms in the Mott-Hubbard picture for the MIT.¹⁶ Since the MIT was observed with partial substitution of Ru by Mn in $\text{Sr}_3\text{Ru}_2\text{O}_7$,^{13,14} one expects that the study of core-level structure may shed light on the nature of doping-induced MIT in this system. Recent results of the x-ray absorption spectroscopy (XAS) taken from Mn-doped $\text{Sr}_3\text{Ru}_2\text{O}_7$ suggest that Mn impurities do not exhibit the same $4+$ valence as Ru but act as $3+$ and the observed MIT is purely electronic.¹⁷ Therefore, it is expected that Ru

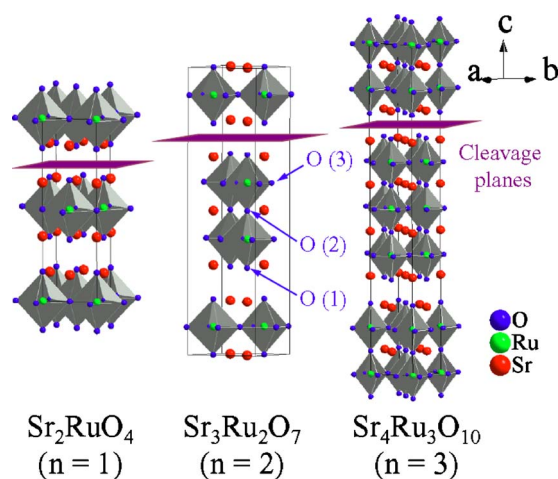


FIG. 1. (Color online) Units cells of Sr_2RuO_4 ($I4/mmm$), $\text{Sr}_3\text{Ru}_2\text{O}_7$ (Pbn), and $\text{Sr}_4\text{Ru}_3\text{O}_{10}$ ($Pbam$). The different sites of oxygen ions in $\text{Sr}_3\text{Ru}_2\text{O}_7$ are labeled. The surfaces were created by cleaving the crystals between two SrO layers without breaking RuO_6 octahedra.

core-level XPS spectra may give further indication about doping-induced multiple Ru valences (Ru^{4+} and Ru^{5+}) and, more importantly, the nature of the doping-induced MIT. In addition, one expects that the change in the number n of RuO_6 octahedral layers should affect the electronic structures and the electron correlation in the layered $\text{Sr}_{n+1}\text{Ru}_n\text{O}_{3n+1}$ series. However, the relationship between the changes in the electron correlation strength and the changes in the dimensionality (n) as well as the doping effect is far from clear. In this study, we used XPS to systematically investigate both the dimensionality and doping effects on the electronic structure and correlation in the $\text{Sr}_{n+1}\text{Ru}_n\text{O}_{3n+1}$ series ($n=1, 2,$ and 3) and Mn-doped $\text{Sr}_3(\text{Ru}_{1-x}\text{Mn}_x)_2\text{O}_7$ system ($x=0.0, 0.1,$ and 0.2).

II. EXPERIMENTS

The single crystals of $\text{Sr}_{n+1}\text{Ru}_n\text{O}_{3n+1}$ ($n=1, 2,$ and 3) and Mn-doped $\text{Sr}_3(\text{Ru}_{1-x}\text{Mn}_x)_2\text{O}_7$ ($x=0, 0.1,$ and 0.2) were grown by the floating zone technique.^{8,9,13,18,19} The x-ray diffraction on these crystals did not reveal any impurity phase. The samples were cleaved at room temperature in ultrahigh vacuum conditions to form a (001) surface and were immediately transferred into the μ -metal-shielded analysis chamber equipped with a computer controlled low-energy electron-diffraction (LEED) diffractometer and XPS. The crystals were cleaved between two SrO layers without breaking RuO_6 octahedra (see the cleavage planes in Fig. 1). XPS measurements were carried out with a Phoibos-150 hemispherical energy analyzer (from SPECS) by using photons of energy of 1486.7 eV from a Micro-Focus 500 ellipsoidal crystal monochromator with Al $K\alpha$ x-ray source and focusing x-ray spot capabilities. A pass energy of 10 eV was used for the measurements. The overall energy resolution for the XPS spectra is 0.16 eV. The Fermi level (E_F) of a Au sample was measured and used to calibrate the binding energy of all core-level spectra. All the XPS data were measured as the samples were at room temperature ($T=300$ K). The base pressure of our system during the measurements was 2×10^{-10} Torr.

The binding energy, linewidth, and intensity of all measured core levels were determined through the standard fitting procedure. All core-level peaks were fitted to Voigt function, which is a convolution of Lorentzian and Gaussian components. The Lorentzian component accounts for the intrinsic line profile of core-level excitations with finite lifetime while the Gaussian one represents the contributions from other extrinsic broadening such as inhomogeneities in the surroundings of the emitting atoms as well as thermal and instrumental broadening. We used Shirley background profile¹⁹ to fit the background of XPS spectra. The Shirley empirical function has been widely used to take account of the inelastic background of a core-level peak with in a relatively small amount of inelastic scattering. This background profile is proportional to the integrated photoelectron intensity to higher kinetic energy.

III. RESULTS AND DISCUSSION

A. Structures and LEED results

The structure of Sr_2RuO_4 is tetragonal with $I4/mmm$ (Fig. 1) symmetry while the structures of $\text{Sr}_3\text{Ru}_2\text{O}_7$ and $\text{Sr}_4\text{Ru}_3\text{O}_{10}$

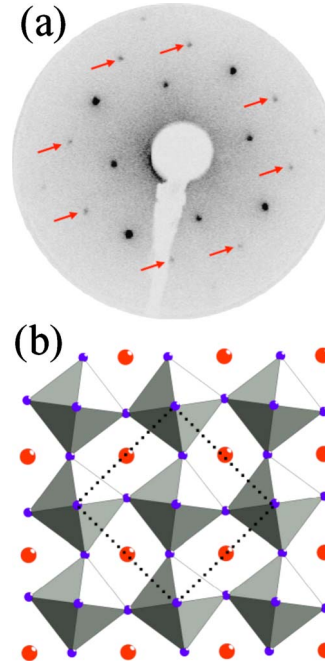


FIG. 2. (Color online) (a) A typical LEED pattern from a freshly cleaved $\text{Sr}_3\text{Ru}_2\text{O}_7$ (001) surface taken at room temperature with electron-beam energy of 77 eV. Fractional order spots with respect to the tetragonal structure are indicated by red arrows. (b) Schematic structure of a single RuO_2 plane. The surface unit cell is shown as a black dashed square. The big red balls represent Sr atoms and the small blue ones at the vortex of the RuO_6 octahedra represent O atoms.

are orthorhombic through rotations about the c axis of the neighboring corner-sharing octahedra within each layer of the double or triple perovskite blocks.^{20,21} However, a recent single-crystal x-ray study suggests that the bulk $\text{Sr}_4\text{Ru}_2\text{O}_7$ can still be modeled by $I4=mmm$ symmetry, where the rotation is represented by the splitting of the equatorial O positions.²² These rotations result in a decrease in the Ru-O-Ru angle in the ab plane to 165° in $\text{Sr}_3\text{Ru}_2\text{O}_7$ and 158° in the middle layers of $\text{Sr}_4\text{Ru}_3\text{O}_{10}$ from the 180° in tetragonal Sr_2RuO_4 . Although the RuO_6 octahedra in these crystals have very similar size, the bond environment of cation Sr changes with number n of RuO_6 octahedral layers. Inside the crystals, Sr has only one kind of bonding environment [Sr-O(1)/Sr-O(3)] in the single-layered Sr_2RuO_4 (Ref. 23) while two kinds of distinct bonding environments [Sr-O(1)/Sr-O(3) and Sr-O(2)/Sr-O(3)] present in both the double²⁴- and triple²⁰-layered compounds (see Fig. 1).

Figure 2(a) shows a typical LEED pattern taken from the cleaved surface of $\text{Sr}_3\text{Ru}_2\text{O}_7$ at room temperature, showing excellent diffraction beams. In addition to the bright spots, there are weak spots (marked by arrows) related to the orthorhombic structure through the alternating in-plane rotation of RuO_6 octahedra about the (001) axis in bulk [see Fig. 2(b)]. Our LEED images confirm that the surfaces of doped and undoped $\text{Sr}_3\text{Ru}_2\text{O}_7$ as well as $\text{Sr}_4\text{Ru}_3\text{O}_{10}$ have $p(1 \times 1)$ structure without surface reconstruction. The fractional spots observed in LEED (see Fig. 2) with a $(\sqrt{2} \times \sqrt{2})R45^\circ$ structure are with respect to the tetragonal structure notation. This

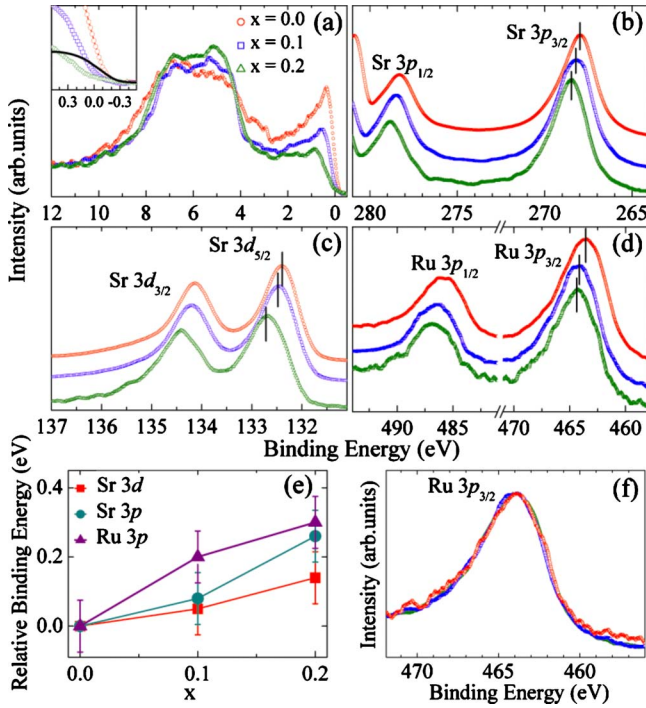


FIG. 3. (Color online) Valence and core-level photoemission spectra of the $Sr_3(Ru_{1-x}Mn_x)_2O_7$ ($x=0.0, 0.1$, and 0.2) measured at $T=300$ K: (a) valence spectra; (b) Sr $3p$; (c) Sr $3d$; (d) Ru $3p$ spectra; (e) energy shifts of Ru $3p$, Sr $3p$, and $3d$ core-level spectra relative to those in $Sr_3Ru_2O_7$ ($x=0.0$) plotted against the doping level; and (f) the Ru $3p_{3/2}$ core level after being shifted for the comparison of line shape. The peak positions are marked by the solid bars. The zoom-in valence spectra close to E_F compared with that taken from a Au sample (black solid curve) are shown in the inset of panel (a).

surface reconstruction corresponds to a bulk soft-phonon mode freezing into a static lattice distortion.²⁵

B. Doping dependence of core-level spectra

Previous XAS (Ref. 17) on $Sr_3(Ru_{1-x}Mn_x)_2O_7$ ($x=0.0$ and 0.1) suggests that the driving mechanism for the observed doping-induced MIT is purely of electronic origin. To verify this, we have performed the XPS study on $Sr_3(Ru_{1-x}Mn_x)_2O_7$. Figure 3 presents the valence band and some characteristic core-level spectra of the $Sr_3(Ru_{1-x}Mn_x)_2O_7$ ($x=0.0, 0.1$, and 0.2). With Mn doping, a clear spectral weight transfer can be seen in the valence spectra [see Fig. 3(a)]. The spectral weight of the quasiparticle band considerably decreases and transfers to higher binding-energy region of $3.0\text{--}10$ eV. This should be associated with the enhanced electron localization with increasing Mn doping and consequently the doping-induced MIT observed in the system. There is yet no clear microscopic understanding for the doping-induced MIT. Structural studies¹⁴ indicate that when the system is doped with Mn the RuO_6 octahedra are compressed along c axis in a Jahn-Teller-type fashion, resulting in the bulking of octahedral layer. Such structural modifications with doping cause a change in the relative energy of

the t_{2g} orbitals and consequently in the transport and magnetic properties.

As shown in Figs. 3(b)–3(d), both Sr and Ru core levels shift to higher binding energy with increasing Mn doping. In particular, Sr and Ru $3p$ core levels exhibit almost identical shifts with doping [see Fig. 3(e)]. Such similar shifts may be attributed to final-state effects due to the reduction in screening to core holes with Mn doping. With the increase in Mn doping, the valence electrons are becoming more localized and reduce their screening to core hole, thus resulting in an increase in apparent binding energy in the core-level spectra. However, as we will discuss below, we also need to take into account the effects of doping-induced change in chemical environment known as initial-state effects.

One important issue for understanding the nature of Mn-doped $Sr_3Ru_2O_7$ is the valence of Mn impurity in the doped compounds. In $Sr_3Ru_2O_7$, the valences of ions are Sr^{2+} , Ru^{4+} , and O^{2-} , which would suggest the substitution of Ru^{4+} with Mn^{4+} upon doping. However, the XAS measurements¹⁷ on the $Sr_3(Ru_{0.9}Mn_{0.1})_2O_7$ suggested that Mn impurities did not exhibit the same $4+$ valence as Ru but acted as $3+$ ones. This conclusion was obtained by comparing the isotropic Mn $L_{2,3}$ -edge XAS data from $Sr_3(Ru_{0.9}Mn_{0.1})_2O_7$ with these from stoichiometric Mn oxides of known valences such as $LaMnO_3$ and $Sr_3Mn_2O_7$. If the Mn substituent in $Sr_3(Ru_{1-x}Mn_x)_2O_7$ acts as a Mn^{3+} ion, a substantial charge transition disproportionation of $Mn^{4+} + Ru^{4+} \rightarrow Mn^{3+} + Ru^{5+}$ should exist in the system and the Ru ions in doped samples should be mixed valent with Ru^{4+}/Ru^{5+} . This would result in two components in the Ru core-level spectra associated with Ru^{4+} and Ru^{5+} ion, respectively. As long as these two components have difference in binding energy based on the scenario of initial-state effect, one would expect that the line shape of Ru core spectra varies with doping. As shown in Fig. 3(f) where we shifted the Ru $3p_{3/2}$ peaks measured from the $x=0.1$ and 0.2 samples to lower binding energy in order to line up with the peak of the undoped compound. The Ru $3p_{3/2}$ peaks of these three samples completely overlap, showing no change in line shape with doping. Therefore, there is no indication of multiple Ru valences induced by Mn doping in the core spectra in contrast with the results of x-ray absorption spectroscopy. The doping dependence of the Mn $2p$ core-level spectra, with $2p_{1/2}$ at ~ 653 eV and $2p_{3/2}$ at ~ 642 eV, is shown in Fig. 4(a) (see the inset). Because of the relatively weak Mn XPS signal, we are unable to resolve any change in Mn core levels with doping.

As we have mentioned above, Mn doping induces a MIT in $Sr_3Ru_2O_7$ (Refs. 13 and 14) which should be reflected in the Ru $3d$ spectral evolution. In fact, the Ru $3d$ spectra exhibit strong doping dependence. As shown in Fig. 4(a), both Ru $3d_{3/2}$ and $3d_{5/2}$ core levels show double peaks, one labeled as “screened (s)” peak with lower binding energy and the other labeled as “unscreened (u)” peak with higher binding energy. For $Sr_3Ru_2O_7$, the s peak of Ru $3d_{5/2}$ is located at 280.76 eV and the u one at 282.13 eV. The separation of these two peaks in both Ru $3d_{3/2}$ and $3d_{5/2}$ core levels is about 1.47 eV for the undoped sample and 1.33 eV for both doped samples. These peaks in the Ru $3d$ spectra shift to higher binding energy with doping. The spectral weight of the s peak decreases while the u peak increases with doping.

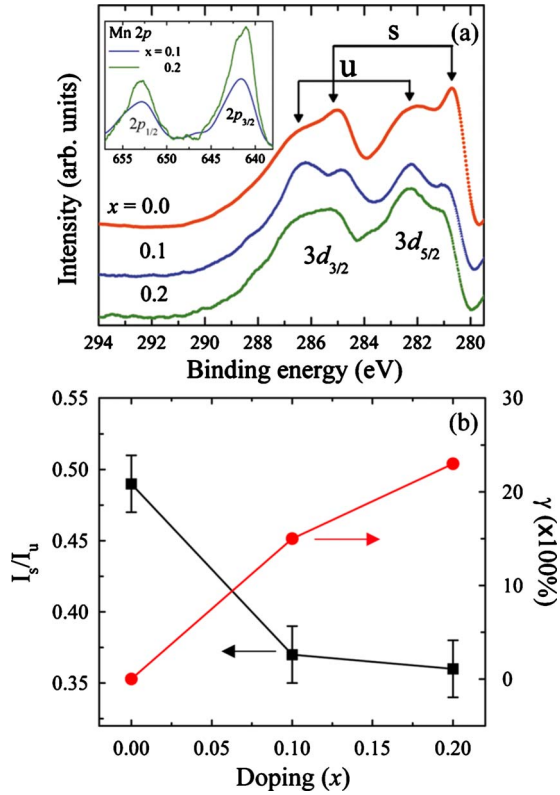


FIG. 4. (Color online) (a) Doping dependence of Ru $3d$ spectra with screened (s) and unscreened (u) components taken from Mn-doped $\text{Sr}_3\text{Ru}_2\text{O}_7$ and (b) intensity ratio of the fitted s and u peaks of the Ru $3d_{5/2}$ and the relative change in the first moment of the intensity-weighted average energy vs Mn doping (see details in text). The inset shows the doping dependence of Mn $3p$ core-level spectra.

The broad u peak is the satellite (referred to as shake-up) due to particle-hole excitations in the presence of the one-particle-hole state. Generally, the intensity of satellites is directly proportional to the degree of electron localization, thus providing a signature for the MIT in a system.

To gain insight into the doping dependence, the spectra were analyzed through standard core-level fitting by assuming that both Ru $3d_{3/2}$ and $3d_{5/2}$ core levels exhibit two-peak structure. Peak positions, widths, and intensities were determined by fitting with Voigt function after Shirley background subtraction. Peak fittings of the Ru $3d_{3/2}$ and $d_{5/2}$ spectra into two-peak structure gave a reasonably good fit to the experimental data. The Lorentzian component, which represents the excitation spectra of core-level states with finite lifetime, was found to be the dominant one for s peaks. The fitting for u peaks contains significant Gaussian broadening. The obtained relative intensity ratio of the u and s component of the Ru $3d_{5/2}$ core level as a function of Mn-doping concentration is plotted in Fig. 4(b). The relative intensity ratio systematically decreases as the Mn concentration increases. This behavior is correlated with that of the spectral weight of the quasiparticle spectra in valence band with doping, suggesting the gradual enhancement of electron localization toward MIT. This behavior is also consistent with the results of the measured transport properties, including Mn-doping-induced MIT.^{13,14}

In order to further understand the nature of these Ru $3d$ core spectra, we have calculated the first moment of the intensity-weighted average binding energy vs Mn doping.^{26,27} According to the basic sum rules for all excitations which generate both the main core-level peak and the associated shake-up satellites in core-level spectra, the first moment of the intensity-weighted energy distribution equals the single-particle Hartree-Fock eigenenergy, i.e.,

$$E_k^{HF} = \int_{-\infty}^{\infty} \epsilon A(\vec{k}, \epsilon) d\epsilon \approx \sum_i \epsilon_i I_i / \sum_i I_i + \text{continuum}, \quad (1)$$

where $A(\vec{k}, \epsilon)$ is the spectral function in the core-level photoelectron excitations. For a core-level spectrum with discrete main peak and satellites, the integration of the spectral function can be replaced by a simple summation of the intensity (I_i) weighted average energy, where index i refers to different discrete peaks, and the excitation continuum. Changes in E_k^{HF} truly reflect the chemical shifts related to the changes in bonding configurations caused (in this case) by doping. For $\text{Sr}_3(\text{Ru}_{1-x}\text{Mn}_x)_2\text{O}_7$, we can determine E_k^{HF} of the Ru $3d_{5/2}$ core level for different doping concentrations by taking into account both the s and u peaks. For simplicity, we neglect the possible change in the excitation continuum with doping. Figure 4(b) presents the doping dependence of the relative shift γ of E_k^{HF} normalized to the energy difference ΔE between the s and u peak. i.e.,

$$\gamma(x) = [E_k^{HF}(x) - E_k^{HF}(x=0)] / \Delta E, \quad (2)$$

where $\Delta E (= 1.33 \text{ eV})$ is the same for both $x=0.1$ and 0.2 samples from our analysis. For the undoped compound, we have $\Delta E = 1.47 \text{ eV}$, slightly larger than that found in the doped ones. It is shown [see Fig. 4(b)] that γ of E_k^{HF} does increase with increasing doping, thus indicating a chemical shift in the core-level spectra. The increase in the binding energy indicates the enhanced localization of the wave functions of the initial states with doping. Therefore, the determination of $\gamma(x)$, which can be used as an order parameter, reveals the critical doping concentration (x_c) for the metal-to-insulator transition observed in the system.

C. Dimensionality effect on core-level spectra

Figure 5 presents the valence band and core-level spectra of the $\text{Sr}_{n+1}\text{Ru}_n\text{O}_{3n+1}$ ($n=1, 2, \text{ and } 3$). The valence-band spectra display a well-defined Fermi edge for all three crystals. The Ru $3d$ and Sr $3p$ core levels are shown in Fig. 5(b). The positions, linewidth, and relative intensity of these features in both valence and Ru $3d$ exhibit similar change in spectral weight with different numbers of RuO_6 octahedral layers, n . The ratios of the coherent to incoherent part in the valence band and the ratio of the s to u component in the Ru $3d$ core level increase slightly with n . The two ratios show a consistent behavior, indicating the electron correlation effects become smaller as the system gets closer to three dimensional. On the other hand, as shown in Fig. 5(c), the Ru $3p_{1/2}$ (at $485.94.1 \text{ eV}$) and $3p_{3/2}$ (at 463.44 eV) core-level spectra of $\text{Sr}_{n+1}\text{Ru}_n\text{O}_{3n+1}$ ($n=1, 2, \text{ and } 3$) are almost identical. It is worth to notice that the surface of the $n=1$ com-

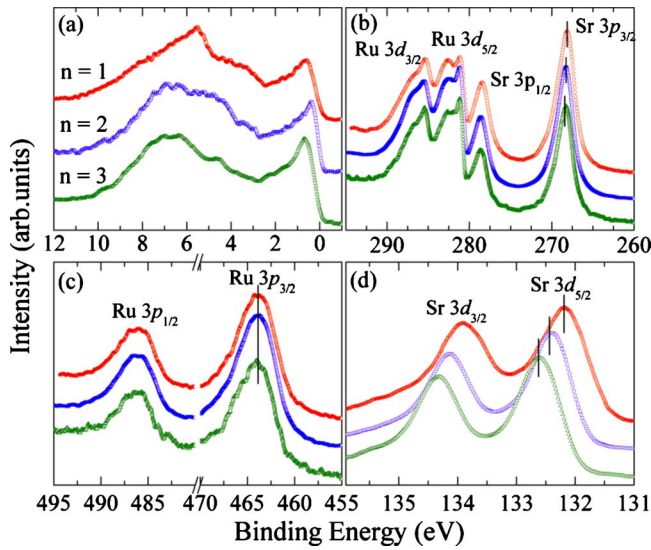


FIG. 5. (Color online) Valence and core-level photoemission spectra of the $\text{Sr}_{n+1}\text{Ru}_n\text{O}_{3n+1}$ ($n=1, 2,$ and 3) measured at $T=300$ K with monochromated $\text{Al K}\alpha$ x-ray source: (a) valence spectra, (b) Ru $3d$ and Sr $3p$, (c) Ru $3p$, and (d) Sr $3d$ core-level spectra. The peak positions are marked by the solid bars. The Fermi edge is calibrated with that of a Au sample.

pound but not the $n=2$ or 3 one has a surface reconstruction. This may give rise to an additional change in the spectral weight of the $n=1$ sample compared to the $n=2$ or 3 compound. Nevertheless, the similar behavior of the Ru core-level spectra is consistent with the similar rigid two-dimensional RuO_6 octahedral layer in all of these layered compounds. It would be interesting to study the similar core levels in SrRuO_3 (i.e., $n=\infty$) which is supposed to be three dimensional rather than quasi-two dimensional. So far there is still no measurement of the core-level spectra from SrRuO_3 single crystal available for comparison.

However, obvious changes are observed in the Sr core-level spectra of the samples with different layered numbers n [see Figs. 5(b) and 5(d)]. In order to compare these three compounds, we plot the shifts of Sr $3p$ and $3d$ as well as Ru $3p$ core spectra, as a function of the number of RuO_6 octahedra layers n relative to $n=1$ in Fig. 6. While Ru core does not change, the Sr cores exhibit increases in binding

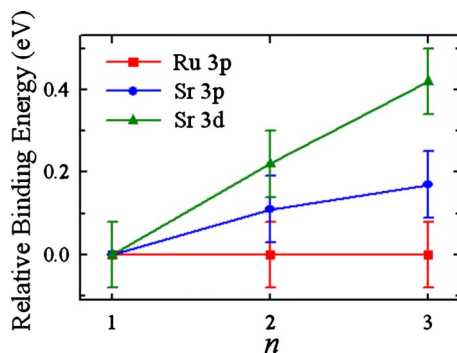


FIG. 6. (Color online) Measured energy shifts relative to the Sr_2RuO_4 ($n=1$) plotted against the number of RuO_6 octahedra layers, n in $\text{Sr}_{n+1}\text{Ru}_n\text{O}_{3n+1}$.

energy with n . Specifically, the Sr $3d$ shallow core levels show stronger n dependence while the shift of the Sr $3p$ core is probably within the range of error bar. Interestingly, the linewidth of $n=1$ sample (~ 0.77 eV) is slightly larger than those from $n=2$ and 3 samples (~ 0.74 eV). This may be attributed to larger surface broadening due to the surface reconstruction of Sr_2RuO_4 .²⁵

In order to understand the different shifts of the binding energy of Sr core-level spectra, it is necessary to examine the structural and bonding evolution of the cations with n in ruthenate. As n increases, the system evolves from quasi-two-dimensional to three-dimensional structure (see Fig. 3). Unlike the Ru ions which are located inside RuO_6 octahedron, the Sr ions has two distinct bonding environments in both $\text{Sr}_3\text{Ru}_2\text{O}_7$ and $\text{Sr}_4\text{Ru}_3\text{O}_{10}$. One bonding environment is the one with Sr-O(1) bond along c axis and Sr-O(3) bond in ab plane, referring to the Sr ions in the cleavage plane (see Fig. 1). The other bonding environment is that of Sr-O(2) bond along c axis and Sr-O(3) bond in ab plane, referring to the Sr ions within the RuO_6 layers. One can expect different chemical shifts due to the different bonding environments as well as the different bond lengths. In particular, the larger shift of Sr $3d$ shallow core levels compared with that of Sr $3p$ indicates a possible participation of $3d$ in bonding. Upon further increasing n , such shifts should gradually diminish as the system approaches a three-dimensional structure such as SrRuO_3 (i.e., $n=\infty$).

IV. SUMMARY

In summary, we have investigated the core-level XPS spectra of layered ruthenates of the $\text{Sr}_{n+1}\text{Ru}_n\text{O}_{3n+1}$ ($n=1, 2,$ and 3) and Mn-doped $\text{Sr}_3\text{Ru}_2\text{O}_7$. We observed that the dimensionality does not affect the Ru but Sr core levels. The Ru $3d$ core-level spectra maintain similar structure for crystals with different octahedral layers (n), suggesting that the chemical bonding environment around Ru ions remains the same for different layered compounds. While the Sr $3d$ shallow core levels shift to higher binding energy with increasing n , indicating a variation in Sr-O bonding with structural evolution. On the other hand, the core levels of $\text{Sr}_3(\text{Ru}_{1-x}\text{Mn}_x)_2\text{O}_7$ show strong dependence of doping concentration (x), revealing the enhanced electron localization with doping toward to MIT. However, the line shape and linewidth of the Ru $3p$ core levels remain identical with doping, showing no sign of multiple Ru oxidation states in Mn-doped system.

ACKNOWLEDGMENTS

This work was supported by U.S. National Science Foundation under Grant No. DMR-0346826. The XPS setup was obtained through the support from U.S. DOD under Grant No. W911NF-07-1-0532. Work at Tulane is supported by DOE under Grant No. DE-FG02-07ER46358 (personnel support), NSF under Grant No. DMR-0645305 (support for equipment), the DOD ARO under Grant No. W911NF-08-C0131 (support for materials), and Research Corporation.

*jjandiz@lsu.edu

- ¹A. P. Mackenzie and Y. Maeno, *Rev. Mod. Phys.* **75**, 657 (2003).
- ²C. Noce, A. Vecchione, M. Cuoco, and A. Romano, *Ruthenate and Rutheno-Cuprate Materials* (Springer, Heidelberg, 2002).
- ³Y. Maeno, H. Hashimoto, K. Yoshida, S. Nishizaki, T. Fujita, J. G. Bednorz, and F. Lichtenberg, *Nature (London)* **372**, 532 (1994).
- ⁴K. Ishida, H. Mukuda, Y. Kitaoka, K. Asayama, Z. Q. Mao, Y. Mori, and Y. Maeno, *Nature (London)* **396**, 658 (1998).
- ⁵K. D. Nelson, Z. Q. Mao, Y. Liu, and Y. Maeno, *Science* **306**, 1151 (2004).
- ⁶S. A. Grigera, R. S. Perry, A. J. SchoTeld, M. Chiao, S. R. Julian, G. G. Lonzarich, S. I. Ikeda, Y. Maeno, A. J. Millis, and A. P. Mackenzie, *Science* **294**, 329 (2001).
- ⁷G. Cao, L. Balicas, W. H. Song, Y. P. Sun, Y. Xin, V. A. Bondarenko, J. W. Brill, S. Parkin, and X. N. Lin, *Phys. Rev. B* **68**, 174409 (2003).
- ⁸Z. Q. Mao, M. Zhou, J. Hooper, V. Golub, and C. J. O'Connor, *Phys. Rev. Lett.* **96**, 077205 (2006).
- ⁹D. Fobes, M. H. Yu, M. Zhou, J. Hooper, C. J. O'Connor, M. Rosario, and Z. Q. Mao, *Phys. Rev. B* **75**, 094429 (2007).
- ¹⁰L. Klein, J. S. Dodge, C. H. Ahn, G. J. Snyder, T. H. Geballe, M. R. Beasley, and A. Kapitulnik, *Phys. Rev. Lett.* **77**, 2774 (1996).
- ¹¹G. Cao, S. McCall, M. Shepard, J. E. Crow, and R. P. Guertin, *Phys. Rev. B* **56**, 321 (1997).
- ¹²S. Nakatsuji and Y. Maeno, *Phys. Rev. Lett.* **84**, 2666 (2000).
- ¹³R. Jin, private communication.
- ¹⁴R. Mathieu, A. Asamitsu, Y. Kaneko, J. P. He, X. Z. Yu, R. Kumai, Y. Onose, N. Takeshita, T. Arima, H. Takagi, and Y. Tokura, *Phys. Rev. B* **72**, 092404 (2005).
- ¹⁵M. Imada, A. Fujimori, and Y. Tokura, *Rev. Mod. Phys.* **70**, 1039 (1998).
- ¹⁶H.-D. Kim, H.-J. Noh, K. H. Kim, and S.-J. Oh, *Phys. Rev. Lett.* **93**, 126404 (2004).
- ¹⁷M. A. Hossain, Z. Hu, M. W. Haverkort, T. Burnus, C. F. Chang, S. Klein, J. D. Denlinger, H.-J. Lin, C. T. Chen, R. Mathieu, Y. Kaneko, Y. Tokura, S. Satow, Y. Yoshida, H. Takagi, A. Tanaka, I. S. Elfimov, G. A. Sawatzky, L. H. Tjeng, and A. Damascelli, *Phys. Rev. Lett.* **101**, 016404 (2008).
- ¹⁸J. Hooper, Z. Mao, R. Perry, and Y. Maeno, *Phys. Rev. Lett.* **92**, 257206 (2004).
- ¹⁹D. A. Shirley, *Phys. Rev. B* **5**, 4709 (1972).
- ²⁰M. K. Crawford, R. L. Harlow, W. Marshall, Z. Li, G. Cao, R. L. Lindstrom, Q. Huang, and J. W. Lynn, *Phys. Rev. B* **65**, 214412 (2002).
- ²¹Q. Huang, J. W. Lynn, R. W. Erwin, J. Jarupatrakorn, and R. J. Cava, *Phys. Rev. B* **58**, 8515 (1998).
- ²²B. Hu, G. T. McCandless, M. Menard, V. B. Nascimento, J. Y. Chan, E. W. Plummer, and R. Jin, *Phys. Rev. B* (to be published).
- ²³M. Braden, A. H. Moudden, S. Nishizaki, Y. Maeno, and T. Fujita, *Physica C* **273**, 248 (1997).
- ²⁴H. Shaked, J. D. Jorgensen, O. Chmaissem, S. Ikeda, and Y. Maeno, *J. Solid State Chem.* **154**, 361 (2000).
- ²⁵R. Matzdorf, Z. Fang, Ismail, J. Zhang, T. Kimura, Y. Tokura, K. Terakura, and E. W. Plummer, *Science* **289**, 746 (2000).
- ²⁶B. I. Lundqvist, *Phys. Kondens. Mater.* **6**, 193 (1967); **6**, 206 (1967); **7**, 117 (1968); **9**, 236 (1969).
- ²⁷H.-J. Freund and E. W. Plummer, *Phys. Rev. B* **23**, 4859 (1981).